HHS Public Access

Author manuscript

Cell Rep. Author manuscript; available in PMC 2019 February 06.

Published in final edited form as:

Cell Rep. 2018 December 26; 25(13): 3869–3883.e4. doi:10.1016/j.celrep.2018.11.099.

Replisome Dynamics and Their Functional Relevance upon DNA Damage through the PCNA Interactome

Mrinal Srivastava[1,3], **Zhen Chen**[1,3], **Huimin Zhang**[1], **Mengfan Tang**[1], **Chao Wang**[1], **Sung Yun Jung**[2], and **Junjie Chen**[1,4,*]

[1]Department of Experimental Radiation Oncology, The University of Texas MD Anderson Cancer Center, Houston, TX 77030, USA

[2]Department of Molecular and Cellular Biology, Baylor College of Medicine, Houston, TX 77030, USA

[3]These authors contributed equally

[4]Lead Contact

SUMMARY

Eukaryotic cells use copious measures to ensure accurate duplication of the genome. Various genotoxic agents pose threats to the ongoing replication fork that, if not efficiently dealt with, can result in replication fork collapse. It is unknown how replication fork is precisely controlled and regulated under different conditions. Here, we examined the complexity of replication fork composition upon DNA damage by using a PCNA-based proteomic screen to uncover known and unexplored players involved in replication and replication stress response. We used camptothecin or UV radiation, which lead to fork-blocking lesions, to establish a comprehensive proteomics map of the replisome under such replication stress conditions. We identified and examined two potential candidate proteins WIZ and SALL1 for their roles in DNA replication and replication stress response. In addition, our unbiased screen uncovered many prospective candidate proteins that help fill the knowledge gap in understanding chromosomal DNA replication and DNA repair.

Graphical Abstract

*Correspondence: jchen8@mdanderson.org.

AUTHOR CONTRIBUTIONS

M.S. and J.C. conceived the project. M.S., Z.C., H.Z., M.T., and C.W. performed the experiments. S.Y.J. helped with mass spectrometry experiments. M.S. and J.C. wrote the manuscript with input from all authors.

SUPPLEMENTAL INFORMATION

Supplemental Information includes seven figures and seven tables and can be found with this article online at https://doi.org/10.1016/j.celrep.2018.11.099.

DECLARATION OF INTERESTS

The authors declare no competing interests.

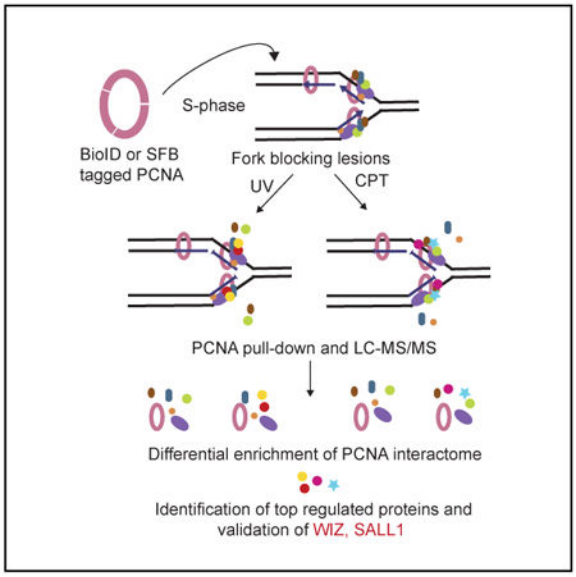

In Brief

Srivastava et al. used unbiased PCNA-centered approaches to construct landscapes of replisome complexes with or without replication stress. These findings uncover many known and previously unexplored proteins that are potentially important for the resolution of two different types of replication fork-blocking lesions.

INTRODUCTION

DNA replication in eukaryotic cells requires dynamic and synergistic action of a plethora of proteins to accurately duplicate the genome. This includes, but is not limited to, precise control of replication origin activation, initiation and ensuring fidelity at replication fork, and restoration of epigenetic regulatory marks. Because DNA replication is spatiotemporally regulated in higher eukaryotes, the composition of the replisome may vary among forks depending on chromatin context, DNA sequence, three-dimensional (3D) nuclear domains, replication timing, and distinct types of fork barriers (Goren et al., 2008; Pope et al., 2014; Zeman and Cimprich, 2014). Despite advances in the field, we still do not fully understand the mechanisms underlying the regulation of chromosomal replication in humans.

Several techniques have been developed in the past decade to uncover and examine proteins that function at replication fork under different conditions (Ohta et al., 2002; Smith et al., 1994), but they each have limitations. Techniques such as immunofluorescence and chromatin immunoprecipitation have been used to determine proteins at replication forks. However, it is challenging to use these techniques to detect ancillary factors that get recruited transiently or only under specific conditions because of their modest sensitivity. Additionally, mammalian cells lack highly specific replication origins with defined primary sequences. Thus, isolation of proteins on nascent DNA (iPOND) has been developed recently to study replication-associated proteins, especially in mammalian cells (Sirbu et al., 2011, 2012). iPOND uses short labeling of newly synthesized DNA with the thymidine

analog EdU, followed by a click chemistry reaction that facilitates purification of DNA-protein complexes. The resolution attained by iPOND can vary depending upon EdU incorporation timing, the rate of DNA synthesis, and chromatin fragment size (Sirbu et al., 2012). Incorporation of analogous nucleotides in nascent DNA allows an inherent bias toward active and fast-moving forks. In order to assess modifications on a replication fork upon DNA damage and/or when encountering other genomic contexts, we need methods that can detect changes occurring at approaching, stalling, and restarting replication forks. We reason that PCNA (proliferating cell nuclear antigen) may be used as an entry way into these diverse replication forks.

In eukaryotes, PCNA monomers form a toroidal homotrimeric complex that encircles DNA and increases the processivity of polymerases by tethering them to the DNA. PCNA coordinates many processes during DNA replication, including chromatin establishment and remodeling of newly synthesized DNA, preventing origin refiring, sister chromatid cohesion, DNA damage bypass, and DNA repair (Maga and Hubscher, 2003; Mailand et al., 2013; Moldovan et al., 2007). Distinctly, PCNA provides a molecular and structural platform that orchestrates these processes through a wide range of specific, spatiotemporally regulated protein-protein interactions that can be monitored to study replication fork dynamics. Furthermore, because PCNA is present on each and every origin and elongating fork, using a PCNA-based technique to assess replication fork variations would alleviate the bias toward active and fast-replicating regions. Therefore, in present study, we used the purification and identification of PCNA interactomes as a proxy for studying proteins that are involved in replication or in various crucial replication-coupled S-phase functions.

RESULTS

Purification and Profiling of PCNA Interactomes

We used both proximity labeling and direct affinity pull-down to study different replication-associated functional networks and their modulations under different conditions (Figure 1A). Furthermore, we simultaneously analyzed the proteomes for both soluble and chromatin-bound PCNA (Figure 1A).

We fused a BioID (proximity-dependent biotin identification) tag to the N terminus of PCNA and confirmed that HEK293T cells expressing BioID-FLAG-PCNA (referred to as BioID-PCNA here-after) could form characteristic foci in S-phase cells (Figures 1B and 1D). In addition, we also generated a control stable cell line expressing BioID-FLAG-GFP (referred to as BioID-GFP here-after) (Figure 1B). As expected, immunofluorescence staining did not show localization of GFP to replication foci (Figure 1D). We used BioID-GFP HEK293T cells as a negative control for every context used for PCNA purification. We also generated stable cell lines containing SFB-triple-tagged PCNA, in which SFB was similarly fused to the N terminus of PCNA. Individual clones were selected on the basis of the expression and the localization of tagged PCNA to replication foci (Figures 1C and 1E). Furthermore, we found that tagged PCNA was present at replication sites post-DNA damage HEK293T cells stably expressing either BioID- or SFB-tagged PCNA (Figure S1A).

In order to test whether our strategy can specifically and stringently enrich for PCNA-interacting proteins involved in replication and various replication-associated processes, we first performed a study using unsynchronized BioID-PCNA cells. Interestingly, our initial study uncovered many PCNA-interacting partners directly involved not only in replication but also in sister chromatid condensation, chromatin remodeling, cell cycle, and DNA repair (Figures 1F, S1B, and S1C). KIAA0101 (also called PAF15) and clamp loaders, such as RFC1-5 and POLD1 (DNA polymerase δ), were enriched in the purification (Figures 1F, S1B, and S1C). Other important replication and known PCNA-interacting proteins, such as TOP2A, LIG1, PRIM2, RNA-SEH2A/B, and CDK2, were also identified (Figures 1F, S1B, and S1C; Table S1).

During replication, PCNA plays a crucial role in the re-establishment of chromatin and epigenetic marks on the newly synthesized DNA. We identified key PCNA-binding proteins, such as chromatin remodeling factor, histone deacetylase BAZ1B, and DNA methyltransferase DNMT1, in our study (Figure 1F). Direct affinity purification of PCNA also pulled down many known proteins involved in DNA replication (POLD2/3, RAD1, LIG1, DNMT1, KIAA0101, SIVA1, and PARG), cell cycle (CDKN1A, CCNE1, CCNA2, CDK1, and CDK5), and chromatin organization (CHTF18) (Figure S1D; Table S2).

Hence, we successfully and specifically enriched for PCNA-interacting proteins using a BioID and SFB-assisted interactome or neighborhood map.

A Proteomic View of the PCNA Interactome Network in S Phase

Next, we performed BioID-PCNA and SFB-PCNA network analysis in synchronized S-phase cells (Figures S2A and S2B). For proximity labeling experiments, in order to increase the stringency and reduce the noise for the PCNA proteome, experiments were compared with control GFP purifications (Figures S2C and S2D; Table S3). After applying a stringent cutoff to detect significant outliers in a volcano plot ($\log_2$ PCNA/GFP versus $\log_{10}$ p value), we obtained a list of 40–50 proteins in the soluble and chromatin fractions (Table S3). For SFB purifications, a list of high-confidence interacting proteins (HCIPs) was generated as described previously (Chen et al., 2016; Li et al., 2017) (Table S4). Despite the stringent filtering criteria, we could identify RFC proteins (RFC1–5), DNA polymerase delta subunits (POLD1–4), and the replisome complex that contains DNA polymerase epsilon (POLE), DNA-directed primase (PRIM1), and LIG1 (Figure 2A). Clamp loader, RAD17, and the replication initiation factor WDHD1 were also detected (Figure 2A).

CHTF18, DSCC1, and CHTF8, which form trimeric complex and enable the cooperation of replication fork to the establishment of cohesion through PCNA interaction (Senga et al., 2006), were also identified (Figures 2A and 2B). Furthermore, our proteomics data were enriched for several PCNA interactors known to play crucial roles governing the reinstatement of chromatin marks to pre-replicative state, such as SMARCAD1, CHAF1A/B, and TLK1/2 (Klimovskaia et al., 2014; Rowbotham et al., 2011; Shibahara and Stillman, 1999) (Figure 2A). Gene Ontology (GO) analysis confirmed that the most significant 15 pathways corresponding to PCNA-associated proteins encompassed DNA replication, repair, recombination, chromosome organization, cell cycle, nucleic acid metabolism, and synthetic processes (Figure 2B; Table S5).

Many PCNA-binding proteins contain a common PCNA-binding motif, namely, the PIP box, which has a consensus sequence of Q-xx-(L/I/M)-x-x-(F/Y)-(F/Y) (Maga and Hubscher, 2003; Moldovan et al., 2007). Several other PCNA-interacting proteins possess a KA box, K-A-(A/L/I)-(A/L/Q)-x-x-(L/V), or an APIM (AlkB homolog 2 PCNA-interacting motif), characterized by [KR]-[FYW]-[LIVA]-[LIVA]-[KR] (Choe and Moldovan, 2017; Moldovan et al., 2007). Strikingly, many of the PCNA-interacting proteins lack one or two of the core amino acids of these consensus sequences and are still able to bind to PCNA. We examined the presence of the PIP box in proteins or protein complexes obtained from our purification results and selected proteins that have at least three of four conserved residues (Figure 2C). Proteins known to contain a PIP box included RNASEH2B, DNMT1, POLD3, RFC1, KIAA0101, ORC3, LIG1, and RAD17 (Figure 2C). Our analysis also revealed the presence of a putative PIP box in a spectrum of other proteins that were not yet known to be part of the replisome complex or the PCNA interactome such as germinal center kinase family member, SLK (STE20-like serine/threonine-protein kinase) (Figure 2C, highlighted in color). Although our focus here was on proteins containing a putative PIP box, it is worth noting that proteins can still interact with PCNA with more degenerated PIP box or even without one through direct or indirect binding.

Synchronization of cells prior to purification significantly enhanced the depth of replication-associated proteins detected (Figure 2D). Several replicative polymerase subunits, FEN1, LIG1, CHTF8, and SIRT1, were among the proteins that were absent in purification of unsynchronized cells but were specifically enriched in S-phase purification (Figure 2D). Comparison between affinity purification and proximity labeling methods revealed that overlapping proteins identified were known to be the part of the replisome complex (Figure S2F). It is noteworthy that we find that these techniques are complementary and evaluation of their combined datasets can provide broader coverage of replisome complex. We also analyzed the overlap between our data and that of BioGrid and selected iPOND studies (Dungrawala et al., 2015; Lopez-Contreras et al., 2013). Our PCNA proteome data showed significant overlap with iPOND data from two different groups (Figures S2G and S2H; Table S6).

Overall, we found that the PCNA interactome provides an efficient way to study the dynamics of replication fork. More pertinently, we uncovered not only known replication proteins but also proteins involved in chromosome segregation, replication-coupled epigenetic inheritance and cell cycle regulation along with a number of proteins that have not yet been characterized in DNA replication and replication-associated functions.

Dynamics of PCNA Interactome Network upon CPT Treatment in S Phase

In the present study, we were particularly interested in the dynamics of PCNA interactome upon DNA damage. Exposure of cells to camptothecin (CPT) results in a covalently linked topoisomerase I-DNA complex (Top1cc), which acts as a roadblock for advancing replication fork; resolving these lesions in S phase is critical for cell survival (Cliby et al., 2002). We treated S-phase-progressing cells with CPT, performed purifications as described above, and generated a list of HCIPs (for both the soluble and chromatin fractions) by comparing the experimental groups with GFP purification controls (Figures S3A and S3B;

Table S3). HCIP lists were further compared with that of the control (untreated) group and explored for proteins that were exclusively present or changed significantly upon CPT treatment (Figures 3A–3C, S3C, and S3D; Table S3). When we ranked these proteins in order of increasing ratios of CPT versus untreated samples (Figures S3C and S3D), the top changed proteins included 53BP1, CCNA2, KANL3, SALL1, and SMARCAD1 (Figures S3C and S3D). CCNA2 (cyclin-A2) is responsible for cell progression through S phase and entry into mitosis (Yam et al., 2002). Upon DNA damage, cyclin A-CDK2 complex and ATM/ATR initiate intra-S phase checkpoint (Woo and Poon, 2003). As for 53BP1, it has been proposed to protect replication forks upon stress and mediate ATR-CHK1 signaling (Her et al., 2018). Taken together, we can speculate that increased levels of CCNA2 and 53BP1 are an indicator of an active DNA damage response in S phase upon CPT treatment. Presence of CDKN1A (p21) (Figure 3B) further supports this observation, as it has been demonstrated to interact with PCNA and inhibit DNA synthesis upon DNA damage (Waga et al., 1994).

Comprehensive analyses of proteins that were either exclusively present in the CPT-treated group or significantly upregulated showed striking enrichment of epigenetic modifiers or readers (Figures 3B–3D, S3C, and S3D). The most probable explanation is that stalling of replication fork leads to specific chromatin remodeling to recruit downstream repair machineries. One of the proteins significantly enriched in the soluble fraction is NSL complex protein, KANL3 (Figures S3A and S3C), which is involved in acetylation of H4 (Cai et al., 2010). Another enriched protein, SALL1 (Sal-like protein 1), which is a zinc finger-containing transcription repressor, has been predicted to be part of the NuRD histone deacetylase (HDAC) complex (Basta et al., 2017). No direct interaction between PCNA and SALL1 was reported. However, the NuRD complex has been shown to co-localize with replication foci (Lai and Wade, 2011), suggesting a possible role during DNA replication.

Some of the other enriched proteins that may have potential role in replication stress response upon CPT treatment are ZNF362, L3MBTL2, and LRWD1 (Figure 3C). ZNF362 is relatively unexplored protein, but it has been indicated to be a relevant interacting partner of TOP2B (Uusküla-Reimand et al., 2016). Recently, L3MBTL2 (lethal[3]malignant brain tumor-like protein 2), has been demonstrated to facilitate recruitment of RNF168 at sites of DNA lesion (Nowsheen et al., 2018). Finally, LRWD1 (leucine-rich repeat and WD repeat-containing protein 1; also called ORCA) is another interesting protein that has been shown to be not only required for G1-S transition but also regulates timing of origin firing (Miotto et al., 2016).

Dynamics of PCNA Interactome Network upon UV Damage in S Phase

We next investigated the PCNA interactome in the setting of UV damage. UV exposure gives rise to DNA helix-distorting lesions such as 6-4 photoproducts and cyclobutane pyrimidine dimers (Cadet et al., 2005). Unrepaired bulky adducts can trigger NER-independent translesion synthesis (TLS). PCNA plays a central role in TLS and is ubiquitylated at K164 by the RAD18-RAD6 ubiquitin ligase complex upon encountering fork-blocking lesion (Hedglin and Benkovic, 2015). TLS polymerases interact more efficiently with mono-ubiquitylated PCNA, thereby mediating lesion bypass. A list of HCIPs

for the UV treatment group was generated as described earlier (Figures S4A and S4B). Upon sorting proteins on the basis of their fold enrichment changes relative to the control group, we focused on proteins that were exclusively present or enriched (Figures 4A, S4C, and S4D) in the UV group. We found that DNA repair proteins such as UNG, RAD18, APEX1, and POLI were exclusively present in the UV group (Figures 4B, 4C, S4C, and S4D; Table S3). Significant and exclusive presentation of RAD18 in the UV-damage group explicitly indicates replication fork stalling and onset of TLS in the UV group (Figures 4B, 4D, S4A, and S4C). This also implies that our tagged PCNA system can undergo damage-dependent modification just as endogenous PCNA.

Another upregulated protein is BAZ1B (tyrosine-protein kinase BAZ1B) (Figures 4C and S4D), which together with SMARCA5 (i.e., chromatin-remodeling complex WICH), prevents the formation of heterochromatin on nascent DNA and serves as a switch between DNA repair or apoptotic signaling upon genotoxic stresses by regulating phosphorylation of H2AX (Poot et al., 2004). It is also worth noting that H2AX levels were significantly increased in the UV-treated group (Figure S4D). As the basal level of H2AX remains the same in the cells, its enrichment indicates an enhanced interaction of the PCNA-UV proteome to modified H2AX, which further points to activation of ongoing repair.

One of the significantly enriched proteins with an unknown role in replication stress response is RCC1 (regulator of chromosome condensation) (Figure S4C), which prevents premature entry of cells into mitosis before completion of replication (Dasso et al., 1992). Although a direct role of RCC1 in DNA repair is not known, it has been suggested that RCC1 activates nuclear import of 53BP1 following DNA damage (Cekan et al., 2016).

Human oncogene DEK is one of the other highly enriched proteins upon UV damage (Figure S4C). Because of its suggested involvement in regulating double-strand break repair (Smith et al., 2017), it is possible that DEK may be involved in post-replication repair of UV lesions via its effect on promoting homologous recombination.

Other interesting proteins that were specifically enriched as HCIPs of the UV group are SSRP1 (also known as FACT80) and VRK1 (vaccinia-related kinase 1) (Figure 4B). SSRP1 is a part of the FACT (facilitates chromatin transactions) histone chaperone complex, involved in replication/repair-coupled nucleosome alterations, and is an ATM/ATR substrate (Yang et al., 2016). VRK1 is a serine-threonine chromatin kinase that has been shown to be important for cell cycle progression and DNA damage response (Valbuena et al., 2008). Enrichment of VRK1 on the replisome upon UV damage points toward the presence of unexplored substrates of this clinically relevant kinase. In a nutshell, our PCNA interactome results from the UV group not only highlight the presence of well-established UV effector proteins but also feature an array of proteins that might compound crucial functions for this subset of replication stress response.

Comparative Analysis of Replisome Response to Two Different Types of Stresses

Next, we wanted to discern whether the two different types of stresses we used for the present study invoke similar or different PCNA-interacting proteins and replisome patterns. Interestingly, we found that almost all known DNA repair proteins uncovered in the CPT-

versus UV-treated groups were different, and the overlap between them was restricted to established replisome proteins (Figure 5A; Table S3).

One of the most notable changes in the CPT group was the presence of chromatin modifiers and readers, including SALL1, ZBTB2, L3MBTL2, HXD13, and MBD2 (Figures 3D and 5B; Table S3). Among the known DNA damage response proteins, ZBTB2 and L3MBTL2 were present in the CPT group (Figure 5B). However, it is worth noting that their specific role in Top1cc resolution has not been investigated. DNA-protein crosslink (DPC) repair is an emerging area of research in the DNA repair field, and the exact course of events involved in DPC resolution has yet to be determined.

On the other hand, the UV-treated group showed exclusive presence of proteins such as RAD18, POLI, APEX1, UNG, POLB, and RAD23 (Figure 5C; Table S3). Not only are these proteins suggested to be involved in DNA repair, a majority of them have been shown to be part of repair processes that remove UV-induced lesions. Among the interesting unknown proteins that might be important for UV repair are DEK, RCC1, VRK1, and STAR9 (Figure 5C). Thus, these data suggest that we could specifically capture replisome changes occurring upon its encounter with different lesions. SFB-PCNA purification revealed modulation in the NUDT10, NUDT11, ZNF544, CGNL1, ZBTB18, and HMCES upon DNA damage (Figures S5A and S5B; Table S4), however, the weaker and transient nature of interactions of DNA response proteins renders the SFB-PCNA purification method limited compared with BioID-PCNA.

Another subset of proteins are those that become less enriched in PCNA interactome upon DNA damage (Figures S3C, S3D, S4C, and S4D; Table 3). Among the HCIPs, we found nominal reduction in replicative polymerases (POLD, POLE, and POLA), LIG1, FEN1, and cohesion proteins, which was consistent with the levels of PCNA upon DNA damage. Proteins that show drastic reduction, such as STRAP, ELAV1, ARF3, DVL2, and GCN1L1, are not present in HCIPs of either the control or treated group. It is worth pointing out that these proteins were eliminated from HCIPs because of their enrichment in GFP groups and are not present in PCNA interactomes.

WIZ May Direct a Methyltransferase Complex to Non-histone Substrates at the Replication Fork

One interesting protein complex present in proximity labeling groups was the G9a-GLP-WIZ complex. It has been suggested that PCNA loading requires a chromatin context marked by methylation of histone H3 at lysine K56, which is catalyzed by G9a (Yu et al., 2012). In addition, recent studies have demonstrated that WIZ, a multiple zinc finger motif-containing protein, acts as an adaptor for GLP/G9a (also called EHMT1/EHMT2) and is important for their chromatin deposition (Bian et al., 2015; Simon et al., 2015). Moreover, WIZ has been found to be enriched on nascent chromatin by iPOND-mass spectrometry (MS) and has been suggested to downregulate fork speed (Lopez-Contreras et al., 2013). However, exactly how WIZ regulates replication remains poorly understood.

In our MS data, WIZ was specifically enriched in the PCNA-containing chromatin fraction. Furthermore, we show that WIZ indeed forms foci in S-phase cells that can co-localize with

PCNA replication foci (Figure 6A). Moreover, we found that deletion of the putative PIP box in WIZ could not completely abrogate WIZ-PCNA interaction in 293T cells (data not shown). It is possible that WIZ may also bind to PCNA through its interaction with G9a/GLP. To validate recruitment of WIZ to replisome, we used iPOND followed by western blotting analysis. WIZ was detected in pulldown of EdU-labeled DNA followed by a click reaction, and its levels decreased after the thymidine chase, suggesting that WIZ travels with the replication fork (Figure 6B). In order to confirm binding of WIZ to nascent DNA, a pull-down experiment was performed in BrdU-labeled cells. We found enrichment of BrdU-labeled DNA upon WIZ pull-down at 3 and 6 hr after release from the double-thymidine block, further confirming that WIZ can bind to nascent DNA in S-phase cells (Figure 6C).

To study the role of WIZ in replication, we generated WIZ knockout (KO) 293A cells using CRISPR-Cas9 technology (Figure S6A). We found that after few passages, WIZ-KO cells showed a remarkably large number of enlarged nuclei along with the presence of micronuclei (Figure S6B), which is indicative of compromised genome stability. Furthermore, we found a significantly larger number of cells in S phase in WIZ-KO cells than in wild-type control cells (Figures 6D and S6C), suggesting that WIZ is important for the timely progression through S phase. Even in the synchronized culture, WIZ-KO cells spent longer in S phase; however, no cell-cycle arrest was observed (Figure S6D).

The WIZ interacting partner G9a has been reported to directly interact with and is crucial for chromatin recruitment of RPA to damage sites (Yang et al., 2017), which activates the ATR-CHK1 axis of DNA damage response. We examined the sensitivity of WIZ-KO cells with hydroxyurea (HU), ATR inhibitor (ATRi; AZD6738), CHK1 inhibitor (CHKi; LY2606368), and PARP inhibitor (PARPi; olaparib) (Figures S6E-S6H). WIZ-KO cells showed modest sensitivity toward PARPi but not to other compounds at the concentrations tested. We also tested the response of G9a-KO cells following treatment with HU or CHK1i. In agreement with the literature, both of these compounds significantly reduced the viability of G9a-KO cells (Figures S6J-S6L). It is possible that the milder DNA damage sensitivity observed in WIZ-KO cells may be due to the residual amount of G9a complex that can still localize to chromatin and perform its function in S-phase cells.

The G9a-GLP methyltransferase complex is known to be part of the replisome complex (Yu et al., 2012), although its exact function in DNA replication remains a mystery. Using peptide arrays, a recent study determined preferred residues and their sequence context in G9a substrates (Rathert et al., 2008). By using preferred G9a motif as determined by earlier study, we examined their presence in key proteins that are present in the replisome complex and/or are responsible for S phase-specific DNA damage response and found several potential substrates of G9a-GLP-WIZ (Figure 6I). Interestingly, DNA polymerases, such as POLD1 and POLQ, contain a putative methyltransferase substrate motif. There may be many targets of the G9a-GLP complex on the replisome complex, and WIZ, by virtue of its tight DNA binding, may tether the replication fork and methyltransferase complex together.

Furthermore, recruitment of polymerases to the chromatin was examined throughout S-phase progression after synchronization. We found that in control cells, PCNA was recruited to chromatin post-release and decreased after 6 hr (Figure 6E). This trend remained the same

in WIZ-KO cells; however, there was higher residual PCNA despite HU treatment at the zero time point. This could be due to a higher lagging S-phase population observed in WIZ-KO cells (Figure 6E). Interestingly, we found a significantly higher level of TLS polymerase POLH in WIZ-KO cells (Figure 6E), which may indicate increased genomic instability in WIZ-KO cells. This could further explain our results of increased presence of micronuclei and slower replication in WIZ-KO cells (Figures 6D, S6B, and S6C). It would be interesting to validate the possibility of putative methylation of polymerases by the G9a-GLP-WIZ complex and its effect on affinity and processivity.

Role of SALL1 in the Resolution of Top1 Adducts

We were also interested in SALL1, a protein that was significantly upregulated in the chromatin fraction after CPT treatment (Figure 3C). *Sall1* is a member of the *Spalt* ("Spalt-like" [Sall]) family and is critical for organogenesis (Buttgereit et al., 2016). It has been suggested that SALL1 is a putative tumor suppressor, and Townes-Brocks syndrome as well as branchio-oto-renal syndrome can be caused by defects in SALL1 (Kohlhase et al., 1998).

Because SALL1 was specifically enriched in CPT-treated samples in our MS data, we hypothesized that SALL1 may assist in the resolution of TOP1 adducts via opening chromatin and allowing the access of DNA repair factors. To test this possibility, we generated SALL1-KO cells and examined resolution of Top1cc after treatment with CPT (Figures 7A, 7B, and S7A). We stained and quantified Top1cc in wild-type and SALL1-KO cells with the help of an antibody that specifically detects cross-linked topoisomerase but not free topoisomerase (Patel et al., 2016) (Figures 7A and 7B). Interestingly, resolution of Top1cc was significantly slower in SALL1-KO than wild-type cells. There was also concomitant increase in γH2AX foci in the KO cells (Figures 7A and 7C). This observation was also validated by dot-blot analysis, which showed that although the majority of Top1cc was resolved by 5–15 min in control cells, it was retained longer in SALL1-KO cells (Figure 7D). Next, to investigate role of SALL1 in resolution of other protein crosslinks, we treated cells with PARPi and checked levels of trapped PARP1 in a time-dependent manner. We found that resolution of trapped PARP1 is also affected by loss of SALL1 (Figure S7B).

As suggested by the mouse KO studies (Nishinakamura et al., 2001) and the spectrum of genetic disorders caused by mutation in the *SALL1* gene, we found that SALL1 was essential for cellular proliferation (Figure S7C). Because SALL1 appears to play an important role in cell proliferation and genomic instability, we further asked whether SALL1 is frequently mutated in cancer cells. Analysis of The Cancer Genome Atlas (TCGA) dataset showed that SALL1 is frequently mutated in different cancer types, with the highest being in the human skin cutaneous melanoma (20%–25%) (Figure S7D). Furthermore, we compared SALL1 mutation frequency with known melanoma protein markers such as BRAF, NRAS, and TP53. SALL1 mutation frequency was among the highest mutated genes just after BRAF and NRAS (Figure S7E).

SALL1 has been shown to bind to hmeC in cells and regulate transcription (Xiong et al., 2016). In agreement, we also found that SALL1 could specifically pull down hmeC DNA, unlike ZnF3-deleted SALL1 (Figure 7E). We did not observe any enrichment for BrdU-positive DNA upon SALL1 pull-down with or without CPT treatment (data not shown),

which supported our hypothesis that SALL1 does not bind directly to nascent DNA but may be recruited to the stalled replication fork. An earlier study showed that levels of hmeC increase in cells upon replication stress, which helps in recruiting DNA damage sensors (Kafer et al., 2016). Thus, we tested whether loss of SALL1 could affect hmeC levels in cells with or without treatment with CPT. We found that levels of hmeC did not increase noticeably upon CPT treatment, and no difference was observed in its levels throughout the experimental time period (Figure 7F). Because hmeC is present physiologically throughout chromosomes, it is possible that localized changes of hmeC at or near sites of replication stress may be difficult to detect using the slot-blot assay. Collectively, our results suggest that SALL1 is important for cell proliferation and may have a role in DPC repair, which remains to be explored.

DISCUSSION

PCNA is a master regulator of replication-associated S-phase processes. No other protein known to date can rival PCNA's capacity to associate with so many interacting partners and orchestrate events that safeguard the genome during replication and replication stress (Choe and Moldovan, 2017; Moldovan et al., 2007). In this study, we used this unique ability of this "maestro" (Moldovan et al., 2007) to study dynamic changes in the composition of the replication fork under different DNA-damaging conditions. Upon encountering DNA lesions, the progressing replication fork slows down or is completely halted until the damage is cleared. For example, CPT treatment can slow the pace of the moving replication fork by half within minutes of treatment (Sugimura et al., 2008). Under these conditions, scoring replication proteins through nucleotide incorporation-based methods may not provide a complete picture of changes in fork composition.

A methodically regulated turnover of proteins occurs on replication fork from origin recognition, origin firing to replication in early, mid, and late S-phase cells. In the present study, we analyzed changes in the proteome of both nuclear and chromatin-bound PCNA to ensure that we did not miss any key transient changes occurring during replication fork stalling or even upon dislodging of PCNA from the replication fork due to DNA damage or during purification steps. Our proximity labeling experiments were performed through the entire S phase after damage. Because most of the DNA repair signaling and effector protein interactions are transient, even if proteins have already been displaced from the damage sites, we can still recover them from soluble fractions by virtue of biotin labeling. In a way, this method has advantages because we are not looking at a narrow window of DNA repair process but holistically from lesion recognition to DNA repair and recommencement of replication. Hence, we used collective data from soluble and chromatin fractions to draw models to depict enriched proteins under specific DNA-damaging conditions.

In this study, we used both direct affinity and proximity labeling pull-down to study PCNA interactomes and/or proteins present at replication forks. Datasets generated by both of these techniques should be viewed as complementary. Because of differences in their underlying principles, the SFB method is likely to uncover direct and stable protein-protein interactions occurring at the time of harvest, whereas the BioID method is designed to identity proteins in proximity, which may or may not be direct binding or stable interacting proteins.

Moreover, these two methods introduce different artifacts or contaminant proteins, and therefore we must use different ways to eliminate their background noises. Hence, we deliberately did not compare the effectiveness of these two methods head on.

Besides known replisome proteins, we could also identify several proteins that may have a role in replication and replication-associated functions. We found few proteins with a putative PIP box (Figure 2C), such as SLK. Whether SLK indeed interacts with PCNA using the putative PIP box remains to be experimentally verified. Given its role during metaphase re-assembly of the mitotic spindles, it would be interesting to study SLK as a potential PCNA-interacting partner that may function as a regulator for ensuring proper and timely spindle assembly on the replication fork (O'Reilly et al., 2005). Several other proteins worth studying include RCC1, VRK1, WIZ, and DEK. Although its role on the replication fork remains a mystery, we speculate that WIZ, acting as an adaptor of the G9a-GLP methyltransferase, can recruit and guide this methyltransferase complex to methylate specific proteins at the replication fork.

We are only beginning to understand the significance of methylation of non-histone substrates during replication. For example, a polymerase, POLB, is arginine-methylated (R83 and R152) by PRMT6, which significantly enhances its DNA binding and processivity (El-Andaloussi et al., 2006). Methylation of ligase 1 by G9a/GLP enables the recruitment of UHRF1 to replicated DNA (Ferry et al., 2017). We found potential high-affinity G9a substrate motifs in known replisome and replication stress response proteins such as POLD1 and POLQ. In fact, POLQ contains a G9a automethylation mimetic motif (Figure S6I), which corresponds to residues spanning its RAD51 interaction region (Ceccaldi et al., 2015). It would be interesting to test whether anti-recombination activity mediated by this interaction is regulated by methylation. In addition, we found an H3K9-like motif in MLL2 and putative methylation motifs in BLM and CDC45 (Figure S6I). However, the sole presence of these motifs does not make these proteins bona fide methylation substrates, which must be experimentally verified.

By using two different fork-blocking lesions, we found that stalled replication fork may use distinct associations that may be relevant or specific to only particular type of DNA lesion. CPT treatment showed a striking enrichment for chromatin remodelers and reader proteins. It is worthwhile to study the roles of SALL1 along with other top enriched proteins such as LRWD1 and L3MBTL2 in detail to better understand their potential involvement in DPC repair. We contemplate that LRWD1 and L3MBTL2 may be required for new origin firings and recruitment of repair factors adjacent to the stalled replication fork, respectively. In the present study, we showed that SALL1 is required for efficient turnover of Top1cc, but the exact mechanism remains to be deciphered. Because of its similarity to ATRX and SALL4, which have been shown to recruit MRN complex (Netzer et al., 2001; Xiong et al., 2015), it is possible that SALL1 may also help in facilitating recruitment of downstream proteins to sites of DNA damage.

Our study provides proof of principle that studying replisome dynamics through MS of well-known conserved replication proteins under different conditions can give us a complete picture of unknown aspects of this fascinatingly regulated process. Intricate details of origin

recognition, firing, and elongation that have been difficult to monitor in a timely manner can now be explored. MS coupled with ORCs, GINS, Clamp, 9-1-1, RPA, or proteins involved in mid-S-phase (such as RIF1) or late-S-phase events can give us a spatiotemporal view of DNA replication. We anticipate that proximity labeling approaches such as APEX or BioID2, which can be concluded in a much shorter time (minutes to a few hours) (Kim et al., 2016; Lu et al., 2007), along with tagging at the endogenous locus will be used more frequently in the future.

STAR★METHODS

CONTACT FOR REAGENT AND RESOURCE SHARING

Further information and requests for resources and reagents should be directed to and will be fulfilled by the Lead Contact, Junjie Chen (jchen8@mdanderson.org).

EXPERIMENTAL MODEL AND SUBJECT DETAILS

Cell culture, transfection and generation of stable cells—293T and 293A cells were procured from ATCC and grown with Dulbecco's modified Eagle medium (DMEM) containing 10% fetal calf serum (FCS) in 37°C with 5% CO_2. All plasmid transfections were performed using polyethylenimine (PEI). In brief, cells were seeded a day before transfection. For transfection, both 9 μg of PEI and 2 μg of plasmid were diluted in PEI, separately. Diluted PEI was added to the plasmid solution, followed by incubation at room temperature for 15 min, and the mixture was added to cells. The transfection reaction was scaled up or down as needed. For generation of stable cells, transfected 293T cells were diluted, seeded and selected with puromycin. Individual clones were picked and analyzed by western blotting and immunofluorescence staining.

METHOD DETAILS

Plasmids—All guide RNAs used were individually cloned into the BsmBI restriction enzyme site of the LentiCRISPRv2 vector and confirmed by sequencing. Protein expression plasmids were constructed utilizing the GATEWAY cloning system. Briefly, cDNA were purchased, amplified, cloned into pENTER221 and confirmed by sequencing. Entry clones were subsequently recombined to generate N-terminal SFB, MYC and HA-FLAG tag constructs as specified. Deletions were generated by PCR-mediated site-directed mutagenesis. An N-terminal BioID construct was created by cloning PCR-amplified BioID at the N terminus of a pENTER201-PCNA clone, which was further transferred to an N-terminal HA-FLAG destination vector system.

CRISPR Cas9-mediated gene knockout—In brief, respective LentiCRISPRv2 guide RNA plasmids were transfected into 293A cells seeded on 6-well plates along with EGFP plasmid. At 18 h after transfection, cells were sorted using the EGFP signal and seeded at 1 cell per well seeding density in three 96-well plates. Clones were transferred onto 24-well plates. Western blotting was performed to determine knockout (KO) of the desired gene, and selected clones were further verified by sequencing. For the generation of WIZ KO cells, a pool of 4 guide RNAs were used to target different isoforms of the gene. sgRNA squences used for WIZ, SALL1 and G9a are listed in Table S7.

Proximity and affinity mass spectrometry—HEK293T cells containing stable N-terminal BioID, SFB-tagged PCNA and BioID-GFP were expanded and seeded into 150 cm^2 dishes. Three dishes were used for every purification. Cells were synchronized at the G1/S boundary using a double-thymidine block and released into CPT (1 μg/ml)-containing medium where required. For UV damage, a 10 mJ/cm^2 dose was used after cells were released into S phase. All BioID pull downs were independently repeated twice for every condition such as unsynchronous, S-phase, CPT or UV conditions. For BioID labeling, 50 μM biotin was added to media for 16 h. Nocodazole (100 ng/ml) was added to cells to prevent them from entering another round of the cell cycle. Affinity purification was perfomed 2 h after the treatment with UV and CPT. Cells were collected and lysed in 1 × NETN containing protease inhibitors. Chromatin was collected by centrifuging lysate at 13,000 rpm for 30 min. Chromatin was digested by S7 nuclease (10 U/ml) in chromatin extraction buffer containing protease inhibitors for 30 min at 37°C and clarified by centrifuging at 13,000 rpm for 10 min. Both clarified soluble and chromatin fractions were incubated overnight with pre-equilibrated streptavidin beads on rotation at 4°C. Beads were washed 3 times with 1 × NETN buffer with 10 min rotation between every wash. Beads were boiled at 95°C for 10 min in Laemmli buffer and loaded onto 10% SDS-PAGE.

Mass spectrometry analysis was performed in the laboratory of Dr. Jun Qin at Baylor College of Medicine using their standard procedures. Briefly, the pull-down samples were separated by SDS-PAGE and visualized by Coomassie Blue staining. The gel band containing the entire sample was excised into small pieces, destained completely and digested with trypsin at 37°C overnight. The peptides were extracted with acetonitrile and vacuum dried. The samples were reconstituted in loading solution (5% methanol containing 0.1% formic acid) and subjected to nanoscale liquid chromatography coupled to tandem mass spectrometry (nanoLC-MS/MS) analysis with an EASY-nLC 1000 liquid chromatography system (Thermo Fisher, Waltham, MA). A nanoscale reverse-phase high-performance liquid chromatography (HPLC) capillary column was created by packing Reprosil-Pur Basic C18 silica into a fused silica capillary (100 μm inner diameter × ~20 cm length) with a flame-drawn tip. The peptides were separated with a 75-min discontinuous gradient of 4%–26% acetonitrile/0.1% formic acid at a flow rate of 800 nl/min. Separated peptides were directly electro-sprayed into a mass spectrometer (Orbitrap Elite; ThermoFisher, Waltham, MA). The mass spectrometer was set to data-dependent mode, and the precursor MS spectrum was scanned at 375-1300 m/z with 240k resolution at 400 m/z (2×10^6 AGC target). The 25 strongest ions were fragmented via collision-induced dissociation with 35 normalized collision energy and 1 m/z isolation width and detected by using an ion trap with 30 s of dynamic exclusion time, 1×10^4 AGC target and 100 ms of maximum injection time.

The MS raw data were searched in Proteome Discoverer 1.4 (ThermoFisher, Waltham, MA) with Mascot algorithm 2.4 (Matrix Science, Boston, MA). The Human UniProt FASTA database (October 2015) containing 70,097 entries was searched. Dynamic modifications included acetylation of N terminus and oxidation of methionine. The precursor mass tolerance was confined within 20 ppm with fragment mass tolerance of 0.5 Da, and a

maximum of two missed cleavages was allowed. Assigned peptides were filtered with a 1% false discovery rate using percolator validation.

We processed the protein-protein interactions analysis for tandem affinity purification following the two steps described in previous papers (Chen et al., 2016; Li et al., 2017). Briefly, the identified proteins and corresponding peptide spectrum matches (PSMs) were subjected to assessment using the CRAPome methodology. We used 90 tandem affinity purification (TAP)-MS data with randomly selected baits as the negative controls. An FC-B score from CRAPome analysis of higher than 2 was taken as the threshold for potential binding proteins. Then, to assess the specificity of protein-protein interaction, we compared the TAP-MS data with HEK293T whole-cell lysis as the background subtraction. Through comparison with this global expression background, proteins that were enriched above the average fold enrichment following the TAP-MS procedure were included in HCIP lists. To identify the significantly enriched proteins in the BioID experiment, we compared the list obtained using BioID-PCNA to the list obtained using control BioID-GFP. The PSMs for each protein were normalized to the total PSMs of that MS run. Then the ratios between BioID-PCNA and BioID-GFP were calculated and statistically analyzed with a t test. Volcano plots were plotted with the log2 ratio and −log10 of the p value from the t test. With the cutoff curve, significant outliers were the enriched proteins. Network were drawn with the help of either STRING or Genemania database and modified (Szklarczyk et al., 2015; Warde-Farley et al., 2010).

Immunofluorescence staining—When assessing replication foci, cells were grown on coverslips followed by extraction with chilled methanol:acetone (1:1) for 10 min. Following extraction, cells were permeabilized with 0.5% Triton X-100for 5 min, blocked with 2% bovine serum albumin in 1 × TBST buffer and incubated with the respective primary antibody for 30 min at 37°C. Followed by three washes of 5 min each in 1 × TBST, cells were incubated with FITC- or Rhodamine-conjugated secondary antibodies, nuclei were counterstained with Hoechst and the samples were mounted with antifade solution. Visualization was done by confocal or fluorescence microscopy. For all other immmunofluroescence experiments, cells were fixed with 4% paraformaldehyde for 10 min at room temperature, and the rest of the protocol was followed as described above.

Western blotting—Standard protocols for sodium dodecyl sulfate-polyacrylamide gel electrophoresis (SDS-PAGE) and immunoblotting were followed (Henderson and Wolf, 1992). PVDF membrane (Millipore) was used to transfer proteins from polyacrylamide gels. List of antibodies used in the present study is provided above.

Quantification of DPCs and slot blotting—A modified rapid approach to DNA adduct recovery (RADAR) assay was used to detect DPCs as described earlier (Vaz et al., 2016). Briefly, 1-1.2 × 10^6 parental and knockout cells were treated with CPT (1 μM) or olaparib (5 μM) for 1 h. Except for time point 0, after the treatment, media containing CPT or olaparib were removed; cells were washed with 1 × phosphate-buffered saline (PBS) and then allowed to recover in prewarmed DMEM containing 10% FCS. For harvesting cells at specific time points, MB solution (6 M GTC, 10 mM Tris-HCl [pH 6.8], 20 mM EDTA, 4% Triton X-100, 1% sarkosyl and 1% dithiothreitol) was added directly to the plate and cells

were harvested. DNA was precipitated by adding 1 mL of 100% ethanol and was washed three times in wash buffer (20 mM Tris-HCl [pH 6.8], 150 mM NaCl and 50% ethanol) and dissolved in 500 μL of 8 mM NaOH. A small fraction of DNA was treated with proteinase K for 30 min at 50°C and quantified using a NanoDrop spectrophotometer (Thermo Scientific). A sample of 250 or 500 ng of DNA was immobilized on Hybond-N+ membrane (Amersham), UV crosslinked and, after blocking with 5% milk, probed with Top1cc or PARP1 antibody. SYBR green or methylene blue staining was performed to further confirm equal DNA loading. Quantification was done using ImageJ software, Peak area was calculated and normalized with loading controls. Results from three independent repeats were using for quantifications.

For determining hmeC levels, a similar procedure was followed except DNA was heated at 99°C for 10 min and stabilized with an equal volume of chilled 2M ammonium acetate before loading onto the membrane.

Cell cycle and BrdU-FITC/PI staining—For cell cycle analysis, 0.5-1 × 10^6 cells were collected and fixed with ice cold-70% ethanol at 4°C overnight. Cells were recovered by centrifugation, washed and resuspended in 1 × PBS containing propidium iodide (PI; 20 μg/ml) and RNase A (10 μg/ml). Cells were analyzed by flow cytometry. A thymidine block was performed as described (Galgano and Schildkraut, 2006). Hydroxyurea (HU) was also used to arrest cells and analyze their cell cycle progression. Arrested cells were washed and released in normal growth medium and harvested at indicated time points.

For BrdU-FITC/PI staining, cells were pulsed once with BrdU (10 μM, 10 min) and fixed. Cells were denatured in 2 N HCl/0.5% Triton X-100 for 30 min at room temperature followed by neutralization with 0.1 M $Na_2B_4O_7$ (pH 8.5). Cells were recovered by centrifugation and incubated with direct BrdU-FITC conjugated antibody along with RNase A (10 μg/ml) for 30 min at 37°C. Cells were then stained with PI and analyzed by flow cytometry.

Colony-forming assay—A preliminary colony-forming assay was performed for each case in order to determine plating efficiency of every cell line used. In general, 200 cells were seeded in 6-well plates and treated with increasing concentrations of the respective genotoxic compound either for 16-18 h or throughout the course of the experiment as indicated. After ~10 days, plates were washed and stained with crystal voilet solution for visualization of colonies. Colonies were counted and plotted.

iPOND-Western blotting—iPOND was performed as described previously (Sirbu et al., 2012). In brief, cells were pulsed with EdU (10 μM, 10 min), fixed and permeabilized, a click reaction was performed (except in the case of the no-click-reaction control), the cells were sonicated and then pulldown using streptavidin beads was performed. Thymidine chase was performed after EdU labeling by washing and incubating cells with 2 mM thymidine for 15 min. After pulldown, beads were washed 5 times as described previously (Sirbu et al., 2012). Crosslinking was reversed by boiling the samples for 20 min at 95°C. The samples were loaded on SDS-PAGE and analyzed by western blotting using specified antibodies.

Immunoprecipitation and pulldown—For pulldown, cells were lysed in chilled 1 × NETN supplemented with protease inhibitors and incubated on ice for 30 min. Lysate was cleared by centrifugation, and buffer-equilibrated streptavidin beads were added and incubated by rotation at 4°C for 2 h. Proteins were eluted from beads by boiling in 2 × Laemmli buffer and loaded onto SDS-PAGE. Western blotting was conducted using specified antibodies.

For chromatin immunoprecipitation, 2×10^6 cells were incubated with BrdU (20 μM, 15 min) at specific time points after their release from cell cycle arrest. After BrdU labeling, cells were fixed with formaldehyde (1%) and quenched by addition of glycine (125 mM). Cells were collected, lysed in FA140 buffer (50 mM HEPES KOH [pH 7.5], 140 mM NaCl, 1 mM EDTA [pH 8.0], 1% Triton X-100 and 0.1% sodium deoxycholate) supplemented with protease inhibitors. Samples were sonicated to obtain an average fragment size of 500-700 bp. Immunoprecipitation was performed by adding 5 μg of WIZ antibody or rabbit IgG antibody overnight, and the immunocomplex was captured by 50% protein A agarose followed by washing with high-salt FA buffer (500 mM NaCl). Elution was done using 1% SDS and 100 mM sodium bicarbonate solution. Captured DNA (as well as input DNA) was reverse-crosslinked, purified, precipitated and loaded on the slot blot for analysis. SALL1 and SALL1 ΔZn3 pulldown for hmeC binding was performed in a similar manner, and an SFB tag was used to perform the pulldown.

QUANTIFICATION AND STATISTICAL ANALYSIS

All the experiments such as western blots, slot blots, immunofluorescence staining and others were performed at least 2 times or more unless indicated otherwise. Differences between groups were analyzed by using Student t tests. P values less than 0.05 were considered statistically significant.

DATA AND SOFTWARE AVAILABILITY

The mass spectrometry proteomics data have been deposited to the ProteomeXchange Consortium via the PRIDE partner repository, and the accession number for the MS data reported in this paper is PRIDE: PXD011727.

Supplementary Material

Refer to Web version on PubMed Central for supplementary material.

ACKNOWLEDGMENTS

We thank all the members of the Chen laboratory for their help and constructive discussion. We also thank Ms. Sunita Patterson of the Department of Scientific Publications at the University of Texas MD Anderson Cancer Center for editing the manuscript. This work was supported in part by Cancer Prevention and Research Institute of Texas (CPRIT) (RP160667) and NIH (CA157448, CA193124, CA210929, CA216911, and CA216437) grants to J.C. J.C. also received support from the Pamela and Wayne Garrison Distinguished Chair in Cancer Research. We thank MD Anderson's Flow Cytometry and Cellular Imaging Facility (supported by MD Anderson's NIH Cancer Center Support Grant [P30CA016672]) for their help with the flow cytometry experiments. M.S. received support from an MD Anderson Odyssey postdoctoral fellowship.

REFERENCES

Basta JM, Robbins L, Denner DR, Kolar GR, and Rauchman M (2017). A Sall1-NuRD interaction regulates multipotent nephron progenitors and is required for loop of Henle formation. Development 144, 3080–3094. [PubMed: 28760814]

Bian C, Chen Q, and Yu X (2015). The zinc finger proteins ZNF644 and WIZ regulate the G9a/GLP complex for gene repression. eLife 4, e05606.

Buttgereit A, Lelios I, Yu X, Vrohlings M, Krakoski NR, Gautier EL, Nishinakamura R, Becher B, and Greter M (2016). Sall1 is a transcriptional regulator defining microglia identity and function. Nat. Immunol. 17, 1397–1406. [PubMed: 27776109]

Cadet J, Sage E, and Douki T (2005). Ultraviolet radiation-mediated damage to cellular DNA. Mutat. Res 571, 3–17. [PubMed: 15748634]

Cai Y, Jin J, Swanson SK, Cole MD, Choi SH, Florens L, Washburn MP, Conaway JW, and Conaway RC (2010). Subunit composition and substrate specificity of a MOF-containing histone acetyltransferase distinct from the male-specific lethal (MSL) complex. J. Biol. Chem 285, 4268–4272. [PubMed: 20018852]

Ceccaldi R, Liu JC, Amunugama R, Hajdu I, Primack B, Petalcorin MI, O'Connor KW, Konstantinopoulos PA, Elledge SJ, Boulton SJ, et al. (2015). Homologous-recombination-deficient tumours are dependent on Polθ-mediated repair. Nature 518, 258–262. [PubMed: 25642963]

Cekan P, Hasegawa K, Pan Y, Tubman E, Odde D, Chen JQ, Herrmann MA, Kumar S, and Kalab P (2016). RCC1-dependent activation of Ran accelerates cell cycle and DNA repair, inhibiting DNA damage-induced cell senescence. Mol. Biol. Cell 27, 1346–1357. [PubMed: 26864624]

Chen Z, Tran M, Tang M, Wang W, Gong Z, and Chen J (2016). Proteomic analysis reveals a novel mutator S (MutS) partner involved in mismatch repair pathway. Mol. Cell. Proteomics 15, 1299–1308. [PubMed: 27037360]

Choe KN, and Moldovan GL (2017). Forging ahead through darkness: PCNA, still the principal conductor at the replication fork. Mol. Cell 65, 380–392. [PubMed: 28157503]

Cliby WA, Lewis KA, Lilly KK, and Kaufmann SH (2002). S phase and G2 arrests induced by topoisomerase I poisons are dependent on ATR kinase function. J. Biol. Chem 277, 1599–1606. [PubMed: 11700302]

Dasso M, Nishitani H, Kornbluth S, Nishimoto T, and Newport JW (1992). RCC1, a regulator of mitosis, is essential for DNA replication. Mol. Cell. Biol 12, 3337–3345. [PubMed: 1630449]

Dungrawala H, Rose KL, Bhat KP, Mohni KN, Glick GG, Couch FB, and Cortez D (2015). The replication checkpoint prevents two types of fork collapse without regulating replisome stability. Mol. Cell 59, 998–1010. [PubMed: 26365379]

El-Andaloussi N, Valovka T, Toueille M, Steinacher R, Focke F, Gehrig P, Covic M, Hassa PO, Schär P, Hübscher U, and Hottiger MO (2006). Arginine methylation regulates DNA polymerase beta. Mol. Cell 22, 51–62. [PubMed: 16600869]

Ferry L, Fournier A, Tsusaka T, Adelmant G, Shimazu T, Matano S, Kirsh O, Amouroux R, Dohmae N, Suzuki T, et al. (2017). Methylation of DNA ligase 1 by G9a/GLP recruits UHRF1 to replicating DNA and regulates DNA methylation. Mol. Cell. 67, 550–565.e5. [PubMed: 28803780]

Galgano PJ, and Schildkraut CL (2006). G1/s phase synchronization using double thymidine synchronization. CSH Protoc. 2006, pdb.prot4487. [PubMed: 22485833]

Goren A, Tabib A, Hecht M, and Cedar H (2008). DNA replication timing of the human beta-globin domain is controlled by histone modification at the origin. Genes Dev. 22, 1319–1324. [PubMed: 18443145]

Hedglin M, and Benkovic SJ (2015). Regulation of Rad6/Rad18 activity during DNA damage tolerance. Annu. Rev. Biophys 44, 207–228. [PubMed: 26098514]

Henderson CJ, and Wolf CR (1992). Immunodetection of proteins by Western blotting. Methods Mol. Biol 10, 221–233. [PubMed: 23150313]

Her J, Ray C, Altshuler J, Zheng H, and Bunting SF (2018). 53BP1 mediates ATR-Chk1 signaling and protects replication forks under conditions of replication stress. Mol. Cell. Biol 38, e00472–17. [PubMed: 29378830]

Kafer GR, Li X, Horii T, Suetake I, Tajima S, Hatada I, and Carlton PM (2016). 5-Hydroxymethylcytosine marks sites of DNA damage and promotes genome stability. Cell Rep. 14, 1283–1292. [PubMed: 26854228]

Kim DI, Jensen SC, Noble KA, Kc B, Roux KH, Motamedchaboki K, and Roux KJ (2016). An improved smaller biotin ligase for BioID proximity labeling. Mol. Biol. Cell 27, 1188–1196. [PubMed: 26912792]

Klimovskaia IM, Young C, Strømme CB, Menard P, Jasencakova Z, Mejlvang J, Ask K, Ploug M, Nielsen ML, Jensen ON, and Groth A (2014). Tousled-like kinases phosphorylate Asf1 to promote histone supply during DNA replication. Nat. Commun. 5, 3394. [PubMed: 24598821]

Kohlhase J, Wischermann A, Reichenbach H, Froster U, and Engel W (1998). Mutations in the SALL1 putative transcription factor gene cause Townes-Brocks syndrome. Nat. Genet 18, 81–83. [PubMed: 9425907]

Lai AY, and Wade PA (2011). Cancer biology and NuRD: a multifaceted chromatin remodelling complex. Nat. Rev. Cancer 11, 588–596. [PubMed: 21734722]

Li X, Han H, Zhou MT, Yang B, Ta AP, Li N, Chen J, and Wang W (2017). Proteomic analysis of the human tankyrase protein interaction network reveals its role in pexophagy. Cell Rep. 20, 737–749. [PubMed: 28723574]

Lopez-Contreras AJ, Ruppen I, Nieto-Soler M, Murga M, Rodriguez-Acebes S, Remeseiro S, Rodrigo-Perez S, Rojas AM, Mendez J, Muñoz J, and Fernandez-Capetillo O (2013). A proteomic characterization of factors enriched at nascent DNA molecules. Cell Rep. 3, 1105–1116. [PubMed: 23545495]

Lu P, Vogel C, Wang R, Yao X, and Marcotte EM (2007). Absolute protein expression profiling estimates the relative contributions of transcriptional and translational regulation. Nat. Biotechnol 25, 117–124. [PubMed: 17187058]

Maga G, and Hubscher U (2003). Proliferating cell nuclear antigen (PCNA): a dancer with many partners. J. Cell Sci. 116, 3051–3060. [PubMed: 12829735]

Mailand N, Gibbs-Seymour I, and Bekker-Jensen S (2013). Regulation of PCNA-protein interactions for genome stability. Nat. Rev. Mol. Cell Biol 14, 269–282. [PubMed: 23594953]

Mellacheruvu D, Wright Z, Couzens AL, Lambert JP, St-Denis NA, Li T, Miteva YV, Hauri S, Sardiu ME, Low TY, et al. (2013). The CRAPome: a contaminant repository for affinity purification-mass spectrometry data. Nat. Methods 10, 730–736. [PubMed: 23921808]

Miotto B, Ji Z, and Struhl K (2016). Selectivity of ORC binding sites and the relation to replication timing, fragile sites, and deletions in cancers. Proc. Natl. Acad. Sci. U S A 113, E4810–E4819. [PubMed: 27436900]

Moldovan GL, Pfander B, and Jentsch S (2007). PCNA, the maestro of the replication fork. Cell 129, 665–679. [PubMed: 17512402]

Netzer C, Rieger L, Brero A, Zhang CD, Hinzke M, Kohlhase J, and Bohlander SK (2001). SALL1, the gene mutated in Townes-Brocks syndrome, encodes a transcriptional repressor which interacts with TRF1/PIN2 and localizes to pericentromeric heterochromatin. Hum. Mol. Genet 10, 3017–3024. [PubMed: 11751684]

Nishinakamura R, Matsumoto Y, Nakao K, Nakamura K, Sato A, Copeland NG, Gilbert DJ, Jenkins NA, Scully S, Lacey DL, et al. (2001). Murine homolog of SALL1 is essential for ureteric bud invasion in kidney development. Development 128, 3105–3115. [PubMed: 11688560]

Nowsheen S, Aziz K, Aziz A, Deng M, Qin B, Luo K, Jeganathan KB, Zhang H, Liu T, Yu J, et al. (2018). L3MBTL2 orchestrates ubiquitin signalling by dictating the sequential recruitment of RNF8 and RNF168 after DNA damage. Nat. Cell Biol 20, 455–464. [PubMed: 29581593]

O'Reilly PG, Wagner S, Franks DJ, Cailliau K, Browaeys E, Dissous C, and Sabourin LA (2005). The Ste20-like kinase SLK is required for cell cycle progression through G2. J. Biol. Chem 280, 42383–42390. [PubMed: 16236704]

Ohta S, Shiomi Y, Sugimoto K, Obuse C, and Tsurimoto T (2002). A proteomics approach to identify proliferating cell nuclear antigen (PCNA)-binding proteins in human cell lysates. Identification of the human CHL12/RFCs2-5 complex as a novel PCNA-binding protein. J. Biol. Chem 277, 40362–40367. [PubMed: 12171929]

Patel AG, Flatten KS, Peterson KL, Beito TG, Schneider PA, Perkins AL, Harki DA, and Kaufmann SH (2016). Immunodetection of human topoisomerase I-DNA covalent complexes. Nucleic Acids Res. 44,2816–2826. [PubMed: 26917015]

Poot RA, Bozhenok L, van den Berg DL, Steffensen S, Ferreira F, Grimaldi M, Gilbert N, Ferreira J, and Varga-Weisz PD (2004). The Williams syndrome transcription factor interacts with PCNAto target chromatin remodelling by ISWI to replication foci. Nat. Cell Biol 6, 1236–1244. [PubMed: 15543136]

Pope BD, Ryba T, Dileep V, Yue F, Wu W, Denas O, Vera DL, Wang Y, Hansen RS, Canfield TK, et al. (2014). Topologically associating domains are stable units of replication-timing regulation. Nature 515, 402–405. [PubMed: 25409831]

Rathert P, Dhayalan A, Murakami M, Zhang X, Tamas R, Jurkowska R, Komatsu Y, Shinkai Y, Cheng X, and Jeltsch A (2008). Protein lysine methyltransferase G9a acts on non-histone targets. Nat. Chem. Biol 4, 344–346. [PubMed: 18438403]

Rowbotham SP, Barki L, Neves-Costa A, Santos F, Dean W, Hawkes N, Choudhary P, Will WR, Webster J, Oxley D, et al. (2011). Maintenance of silent chromatin through replication requires SWI/SNF-like chromatin remodeler SMARCAD1. Mol. Cell 42, 285–296. [PubMed: 21549307]

Senga T, Sivaprasad U, Zhu W, Park JH, Arias EE, Walter JC, and Dutta A (2006). PCNA is a cofactor for Cdt1 degradation by CUL4/DDB1-mediated N-terminal ubiquitination. J. Biol. Chem 281, 6246–6252. [PubMed: 16407252]

Shibahara K, and Stillman B (1999). Replication-dependent marking of DNA by PCNA facilitates CAF-1-coupled inheritance of chromatin. Cell 96, 575–585. [PubMed: 10052459]

Simon JM, Parker JS, Liu F, Rothbart SB, Ait-Si-Ali S, Strahl BD, Jin J, Davis IJ, Mosley AL, and Pattenden SG (2015). A Role for Widely Interspaced Zinc Finger (WIZ) in Retention of the G9a Methyltransferase on Chromatin. J. Biol. Chem 290, 26088–26102. [PubMed: 26338712]

Sirbu BM, Couch FB, Feigerle JT, Bhaskara S, Hiebert SW, and Cortez D (2011). Analysis of protein dynamics at active, stalled, and collapsed replication forks. Genes Dev. 25, 1320–1327. [PubMed: 21685366]

Sirbu BM, Couch FB, and Cortez D (2012). Monitoring the spatiotemporal dynamics of proteins at replication forks and in assembled chromatin using isolation of proteins on nascent DNA. Nat. Protoc. 7, 594–605. [PubMed: 22383038]

Smith ML, Chen IT, Zhan Q, Bae I, Chen CY, Gilmer TM, Kastan MB, O'Connor PM, and Fornace AJ, Jr. (1994). Interaction of the p53-regulated protein Gadd45 with proliferating cell nuclear antigen. Science 266, 1376–1380. [PubMed: 7973727]

Smith EA, Gole B, Willis NA, Soria R, Starnes LM, Krumpelbeck EF, Jegga AG, Ali AM, Guo H, Meetei AR, et al. (2017). DEK is required for homologous recombination repair of DNA breaks. Sci. Rep 7, 44662. [PubMed: 28317934]

Sugimura K, Takebayashi S, Taguchi H, Takeda S, and Okumura K (2008). PARP-1 ensures regulation of replication fork progression by homologous recombination on damaged DNA. J. Cell Biol. 183, 1203–1212. [PubMed: 19103807]

Szklarczyk D, Franceschini A, Wyder S, Forslund K, Heller D, Huerta-Cepas J, Simonovic M, Roth A, Santos A, Tsafou KP, et al. (2015). STRING v10: protein-protein interaction networks, integrated over the tree of life. Nucleic Acids Res. 43, D447–D452. [PubMed: 25352553]

Uusküla-Reimand L, Hou H, Samavarchi-Tehrani P, Rudan MV, Liang M, Medina-Rivera A, Mohammed H, Schmidt D, Schwalie P, Young EJ, et al. (2016). Topoisomerase II beta interacts with cohesin and CTCF at topological domain borders. Genome Biol. 17, 182. [PubMed: 27582050]

Valbuena A, López-Sánchez I, and Lazo PA (2008). Human VRK1 is an early response gene and its loss causes a block in cell cycle progression. PLoS ONE 3, e1642. [PubMed: 18286197]

Vaz B, Popovic M, Newman JA, Fielden J, Aitkenhead H, Halder S, Singh AN, Vendrell I, Fischer R, Torrecilla I, et al. (2016). Metalloprotease SPRTN/DVC1 Orchestrates Replication-Coupled DNA-Protein Crosslink Repair. Mol. Cell 64, 704–719. [PubMed: 27871366]

Waga S, Hannon GJ, Beach D, and Stillman B (1994).The p21 inhibitor of cyclin-dependent kinases controls DNA replication by interaction with PCNA. Nature 369, 574–578. [PubMed: 7911228]

Warde-Farley D, Donaldson SL, Comes O, Zuberi K, Badrawi R, Chao P, Franz M, Grouios C, Kazi F, Lopes CT, et al. (2010). The GeneMANIA prediction server: biological network integration for gene prioritization and predicting gene function. Nucleic Acids Res. 38, W214–W220. [PubMed: 20576703]

Woo RA, and Poon RY (2003). Cyclin-dependent kinases and S phase control in mammalian cells. Cell Cycle 2, 316–324. [PubMed: 12851482]

Xiong J, Todorova D, Su NY, Kim J, Lee PJ, Shen Z, Briggs SP, and Xu Y (2015). Stemness factor Sall4 is required for DNA damage response in embryonic stem cells. J. Cell Biol. 208, 513–520. [PubMed: 25733712]

Xiong J, Zhang Z, Chen J, Huang H, Xu Y, Ding X, Zheng Y, Nishina-kamura R, Xu GL, Wang H, et al. (2016). Cooperative Action between SALL4A and TET Proteins in Stepwise Oxidation of 5-Methylcytosine. Mol. Cell 64, 913–925. [PubMed: 27840027]

Yam CH, Fung TK, and Poon RY (2002). Cyclin A in cell cycle control and cancer. Cell. Mol. Life Sci 59, 1317–1326. [PubMed: 12363035]

Yang J, Zhang X, Feng J, Leng H, Li S, Xiao J, Liu S, Xu Z, Xu J, Li D, et al. (2016). The histone chaperone FACT contributes to DNA replication-coupled nucleosome assembly. Cell Rep. 16, 3414.

Yang Q, Zhu Q, Lu X, Du Y, Cao L, Shen C, Hou T, Li M, Li Z, Liu C, et al. (2017). G9a coordinates with the RPA complex to promote DNA damage repair and cell survival. Proc. Natl. Acad. Sci. U S A 114, E6054–E6063. [PubMed: 28698370]

Yu Y, Song C, Zhang Q, DiMaggio PA, Garcia BA, York A, Carey MF, and Grunstein M (2012). Histone H3 lysine 56 methylation regulates DNA replication through its interaction with PCNA. Mol. Cell 46, 7–17. [PubMed: 22387026]

Zeman MK, and Cimprich KA (2014). Causes and consequences of replication stress. Nat. Cell Biol 16, 2–9. [PubMed: 24366029]

Highlights

- PCNA interactome was comprehensively explored to reflect replisome dynamics
- Replisome composition characteristically varies upon encountering different stresses
- WIZ and SALL1 were examined for their roles in DNA replication and stress response

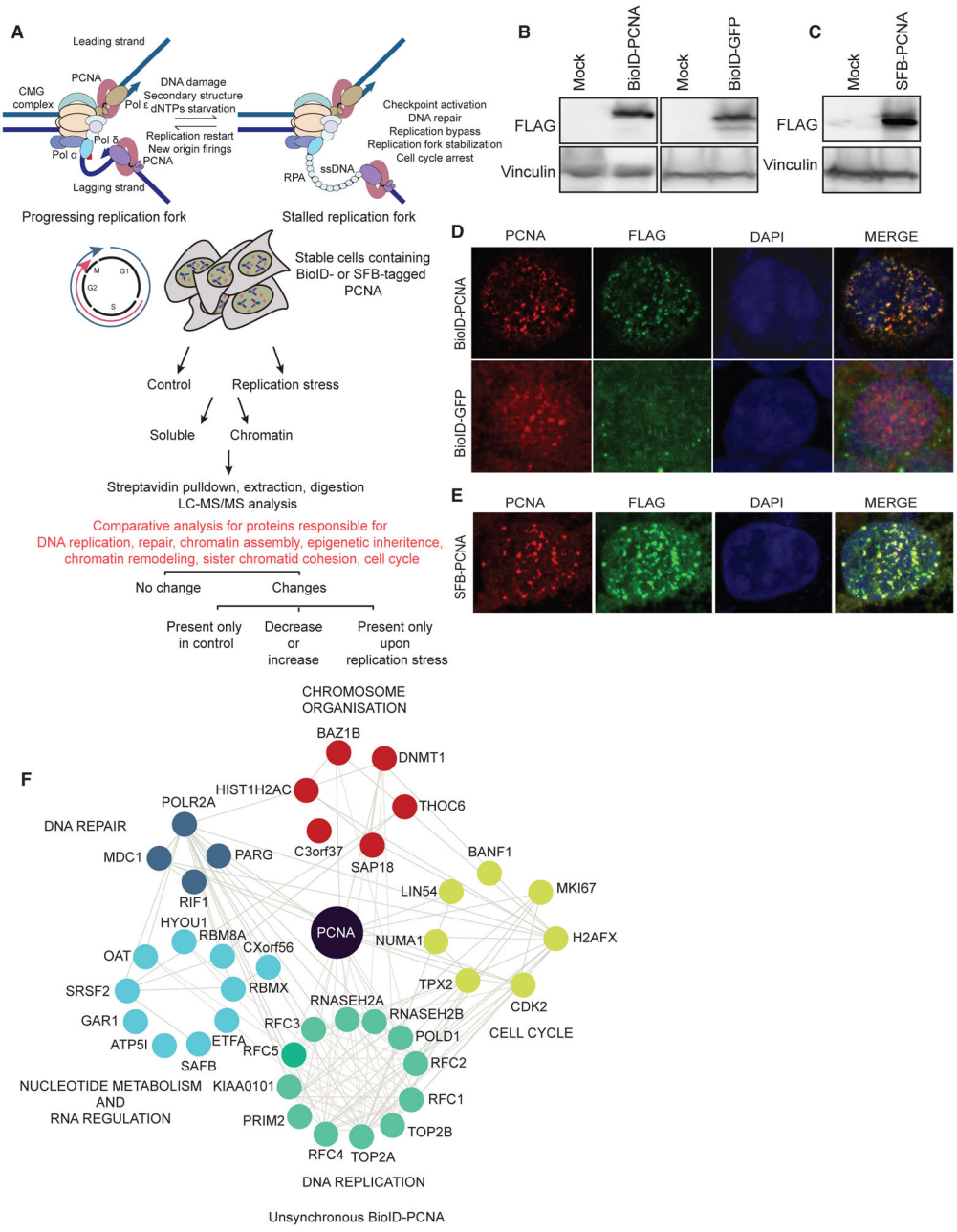

Figure 1. PCNA Interactome as a Strategy to Explore Replication Dynamics

(A) Schematic overview of approaches used to profile replication fork proteins and their modulation via purification of a key replication processivity factor, PCNA.

(B and C) Immunoblotting using the indicated antibodies was conducted to confirm the expression of BioID-FLAG-PCNA (BioID-PCNA) (B) and SFB-PCNA (C) in HEK293T stable clones. Expression of GFP was also confirmed in HEK293T cells stably expressing BioID-FLAG-GFP (BioID-GFP) (B).

(D and E) Immunofluorescence staining was conducted to ensure the correct localization of BioID-PCNA (D) and SFB-PCNA (E) to replication foci. Endogenous PCNA staining

marked replication foci. For proximity labeling purification, BioID-GFP was used as a control.

(F) Network overview of proteins enriched in BioID-PCNA purification in unsynchronized cells. Unsynchronized BioID-PCNA purification was performed twice for both soluble and chromatin fractions along with their respective GFP controls.

See also Figure S1 and Tables S1 and S2.

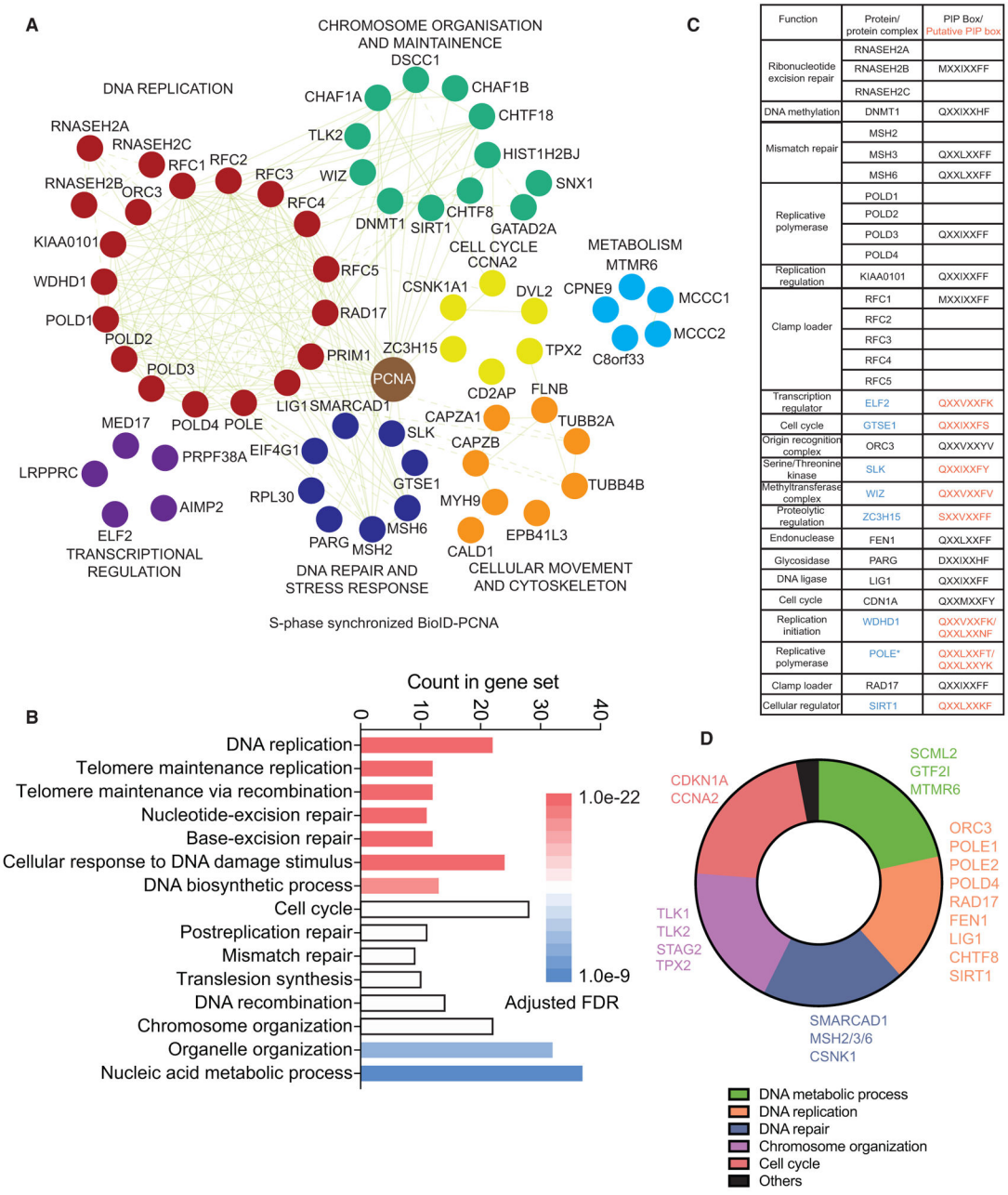

Function	Protein/ protein complex	PIP Box/ Putative PIP box
Ribonucleotide excision repair	RNASEH2A	
	RNASEH2B	MXXIXXFF
	RNASEH2C	
DNA methylation	DNMT1	QXXIXXHF
Mismatch repair	MSH2	
	MSH3	QXXLXXFF
	MSH6	QXXLXXFF
Replicative polymerase	POLD1	
	POLD2	
	POLD3	QXXIXXFF
	POLD4	
Replication regulation	KIAA0101	QXXIXXFF
Clamp loader	RFC1	MXXIXXFF
	RFC2	
	RFC3	
	RFC4	
	RFC5	
Transcription regulator	ELF2	QXXVXXFK
Cell cycle	GTSE1	QXXIXXFS
Origin recognition complex	ORC3	QXXVXXYV
Serine/Threonine kinase	SLK	QXXIXXFY
Methyltransferase complex	WIZ	QXXVXXFV
Proteolytic regulation	ZC3H15	SXXVXXFF
Endonuclease	FEN1	QXXLXXFF
Glycosidase	PARG	DXXIXXHF
DNA ligase	LIG1	QXXIXXFF
Cell cycle	CDN1A	QXXMXXFY
Replication initiation	WDHD1	QXXVXXFK/ QXXLXXNF
Replicative polymerase	POLE*	QXXLXXFT/ QXXLXXYK
Clamp loader	RAD17	QXXIXXFF
Cellular regulator	SIRT1	QXXLXXKF

Figure 2. Enrichment of Replisome Network in Cells Synchronized in S Phase

(A) Protein interaction network for the proteins enriched in BioID-PCNA purification in S-phase cells. The network was constructed with the help of STRING analysis. Results are obtained by two independent repeats of BioID PCNA purifications.

(B) Significant pathways associated with BioID-PCNA purification of S-phase cells as determined by GO analysis. The vertical axis represents the pathway category, and the horizontal axis represents the count in the gene set. The adjusted false discovery rates (FDRs) of the pathways are represented by colors as indicated.

(C) Analysis for presence of a PIP box in enriched BioID-PCNA purifications performed on S-phase cells. Proteins that are known to be part of the PCNA interactome and have an

experimentally verified PIP box are listed in black. Proteins with a putative role in replication are shown in blue, and their corresponding PIP boxes are in red. The asterisk indicates that the site shown is predicted on the basis of conservation of residues with regard to the *Saccharomyces cerevisiae* PIP box.

(D) Pie chart representing top functions for proteins collectively enriched in BioID-PCNA purification using S-phase cells. Some of the proteins that were absent in purification performed on unsynchronized cells are listed, color-coordinated by their respective functions.

See also Figure S2 and Tables S3, S4, S5, and S6.

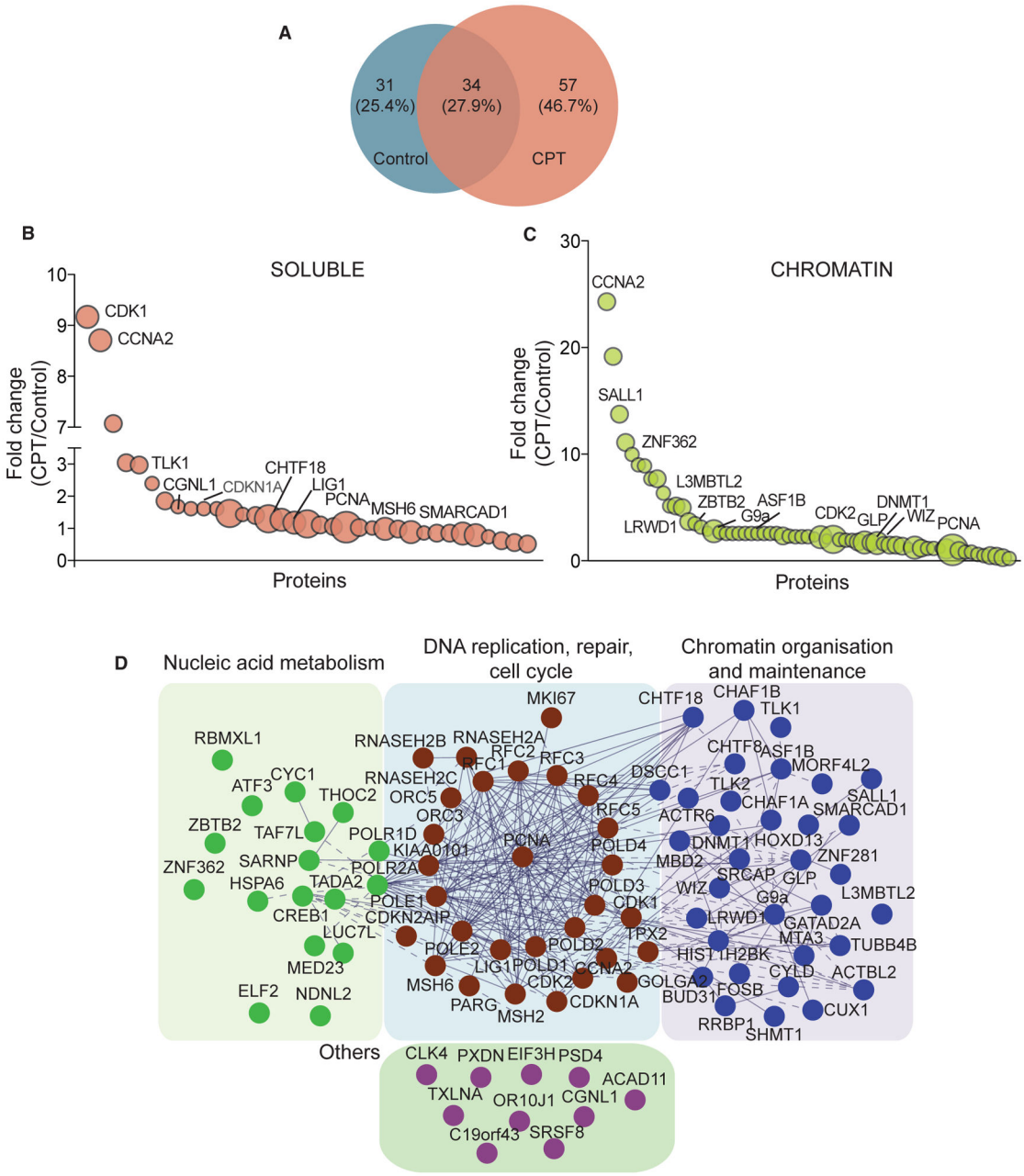

Figure 3. Replisome Dynamics upon CPT Treatment

(A) Venn diagram showing overlap of HCIPs obtained from BioID-PCNA purifications of untreated versus CPT-treated (1 μg/mL) fractions. HCIPs presented were obtained by two independent repeats of BioID PCNA purifications.

(B and C) Relative fold enrichment for the (B) soluble and (C) chromatin fractions of proximity labeling purifications upon treatment with CPT (1 μg/mL) in comparison with mock-treated control. The bubble size shown is relative to their peptide abundance.

(D) STRING network analysis for proteins present or enriched in CPT-treated samples. Proteins are clustered on the basis of their predominant biological function. “Others” represent proteins of miscellaneous or unknown functions.

See also Figure S3 and Table S3.

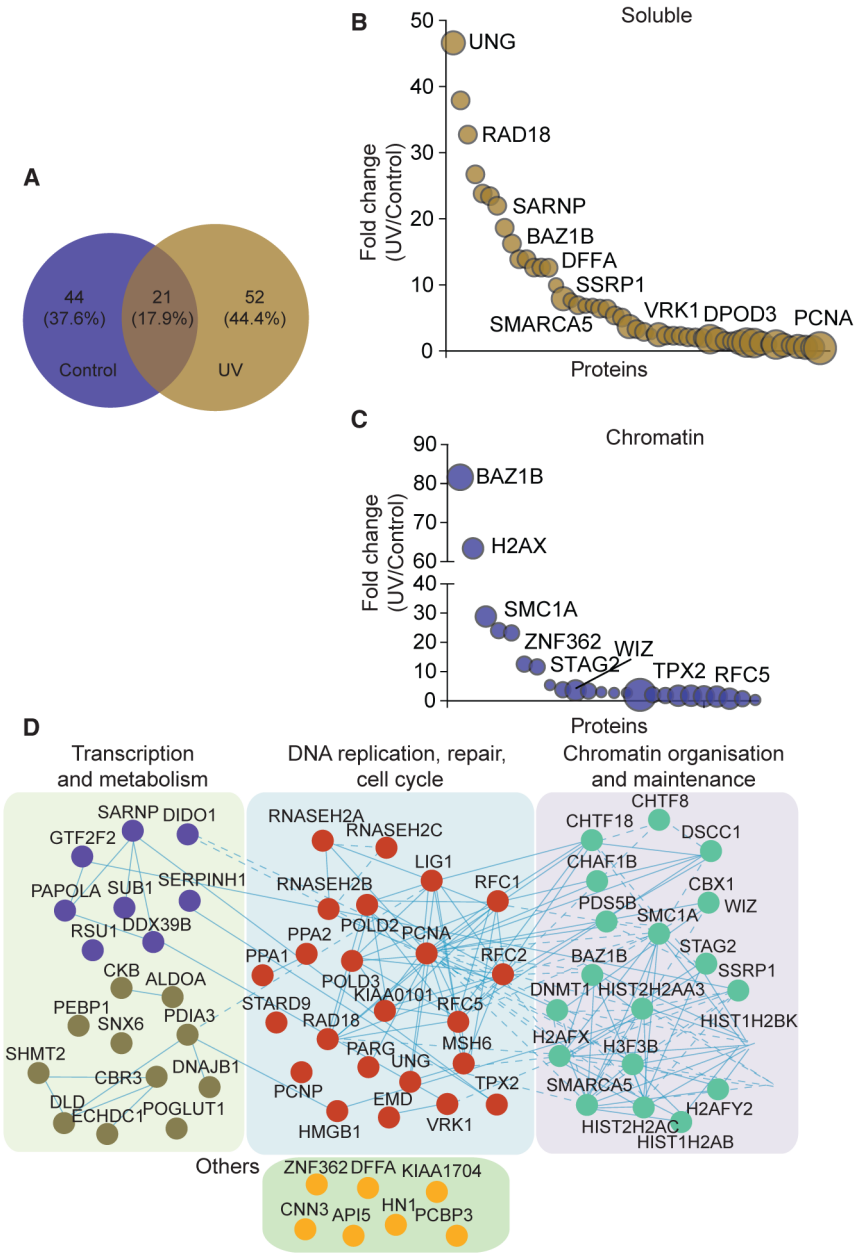

Figure 4. Specific Changes in the Composition of Replication Forks Encountering UV Lesions

(A) Venn diagram showing overlap between BioID-PCNA purifications done using untreated versus UV-treated (10 mJ/cm^2) samples. HCIPs presented were obtained by two independent repeats of BioID PCNA purifications.

(B and C) Relative fold enrichment of proteins found in proximity labeling-MS experiments in the soluble (B) and chromatin (C) fractions upon treatment with UV radiation. The bubble size shown is relative to their peptide abundance.

(D) STRING network analysis for proteins that were exclusively present or enriched in UV-treated samples.

See also Figure S4 and Table S3.

A

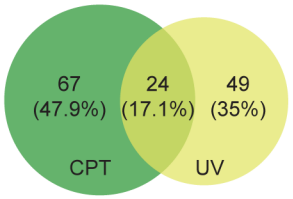

B

Proteins exclusively present in CPT	Known role in replication	Known role in DNA repair
SALL1	X	X
LRWD1	✓	X
L3MBTL2	X	✓
ZBTB2	X	✓
C19ORF43	X	X
CGNL1	X	X
SRSF8	X	X
MBD2	X	X

C

Proteins exclusively present in UV	Known role in replication	Known role in DNA repair
DEK	X	✓
RCC1	X	X
RAD18	X	✓
PARI	✓	✓
PSIP	X	X
RAD23	X	✓
VRK1	X	X
P53	✓	✓
H2AX	X	✓
UNG	X	✓
APEX1	X	✓
BAZ1B	✓	✓
STAR9	X	X
HMCES	X	X
DMAP1	X	X
WDR70	X	X

Figure 5. Comparison of Replisome Dynamics between CPT- and UV-Treated Groups

(A) Venn diagram showing overlap of proteins identified by BioID-PCNA purification in the CPT-treated group versus those in the UV-irradiated group.

(B and C) Proteins that were exclusively enriched in CPT-treated (B) or UV-irradiated (C) samples. Known roles of each listed protein in replication and DNA damage repair are also indicated. A tick sign indicates a positive role in the linked function. An “X” sign indicates that on the basis of the literature, no specific role of this protein in the linked function has been observed.

See also Figure S5 and Tables S3 and S4.

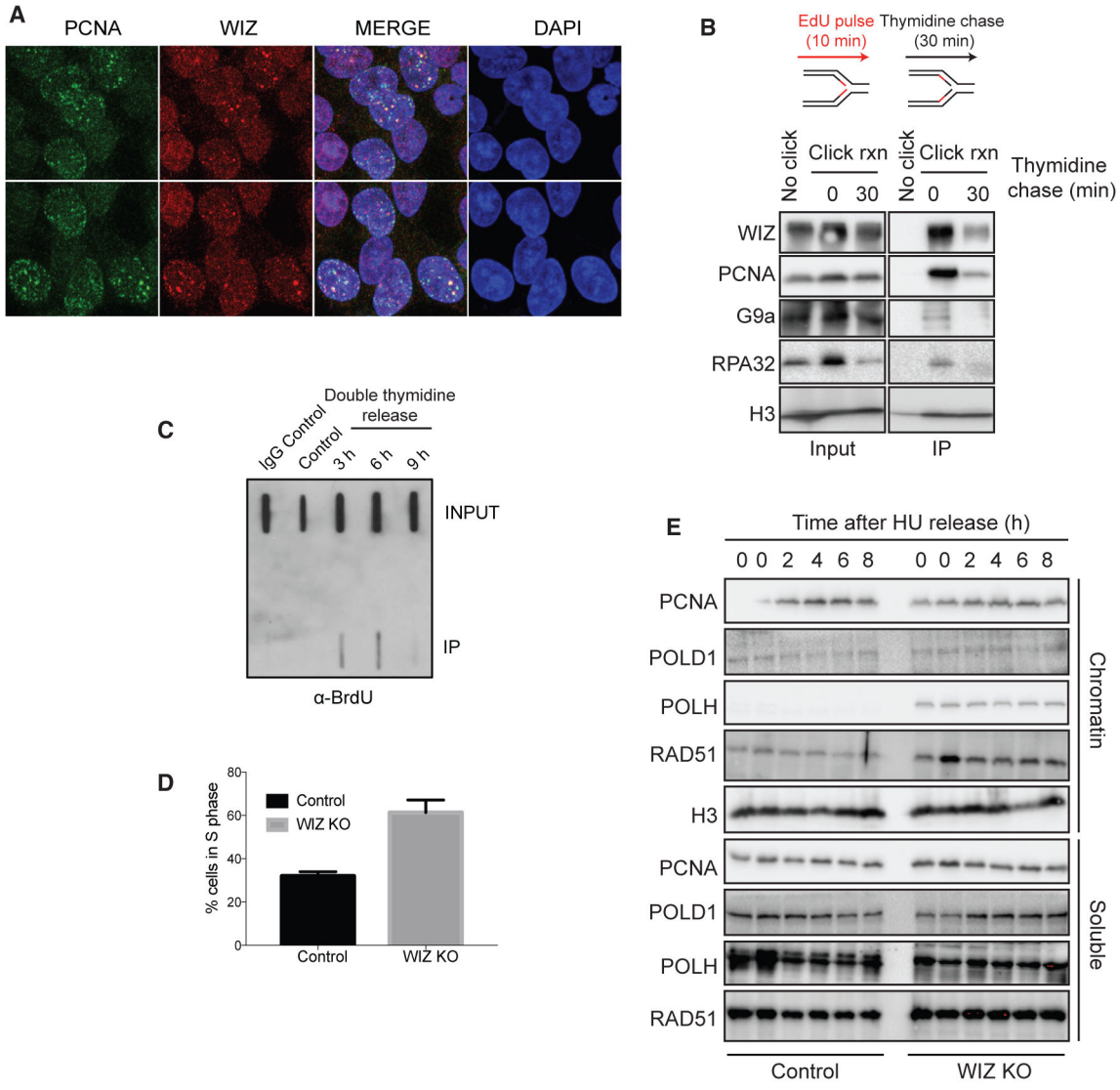

Figure 6. WIZ Plays an Important Role during Replication and Genomic Stability

(A) Immunofluorescence staining showing colocalization of FLAG-WIZ with replication foci, which are marked by PCNA staining.

(B) Western blot analysis of indicated proteins isolated by iPOND. HEK293T cells were pulse-labeled with EdU for 10 min, then chased with thymidine for 30 min, as indicated. In no-click-reaction control samples, biotin azide was replaced with DMSO.

(C) Slot-blot analysis showed that WIZ pulled down BrdU-containing DNA in S-phase cells. Cells were synchronized and pulsed with BrdU for 10 min before collection, and WIZ pull-down was performed using polyclonal WIZ antibody.

(D) Bar graph indicating the percentages of S-phase cells present in wild-type (control) and WIZ-KO cells as determined by BrdU/propidium iodide staining followed by flow cytometry analysis. The SEM from two independent experiments performed in duplicates is indicated.

(E) Western blot analysis of indicated proteins after synchronization and release of 293A WT control and WIZ-KO cells following treatment with HU (2 mM) for 16 hr.

See also Figure S6.

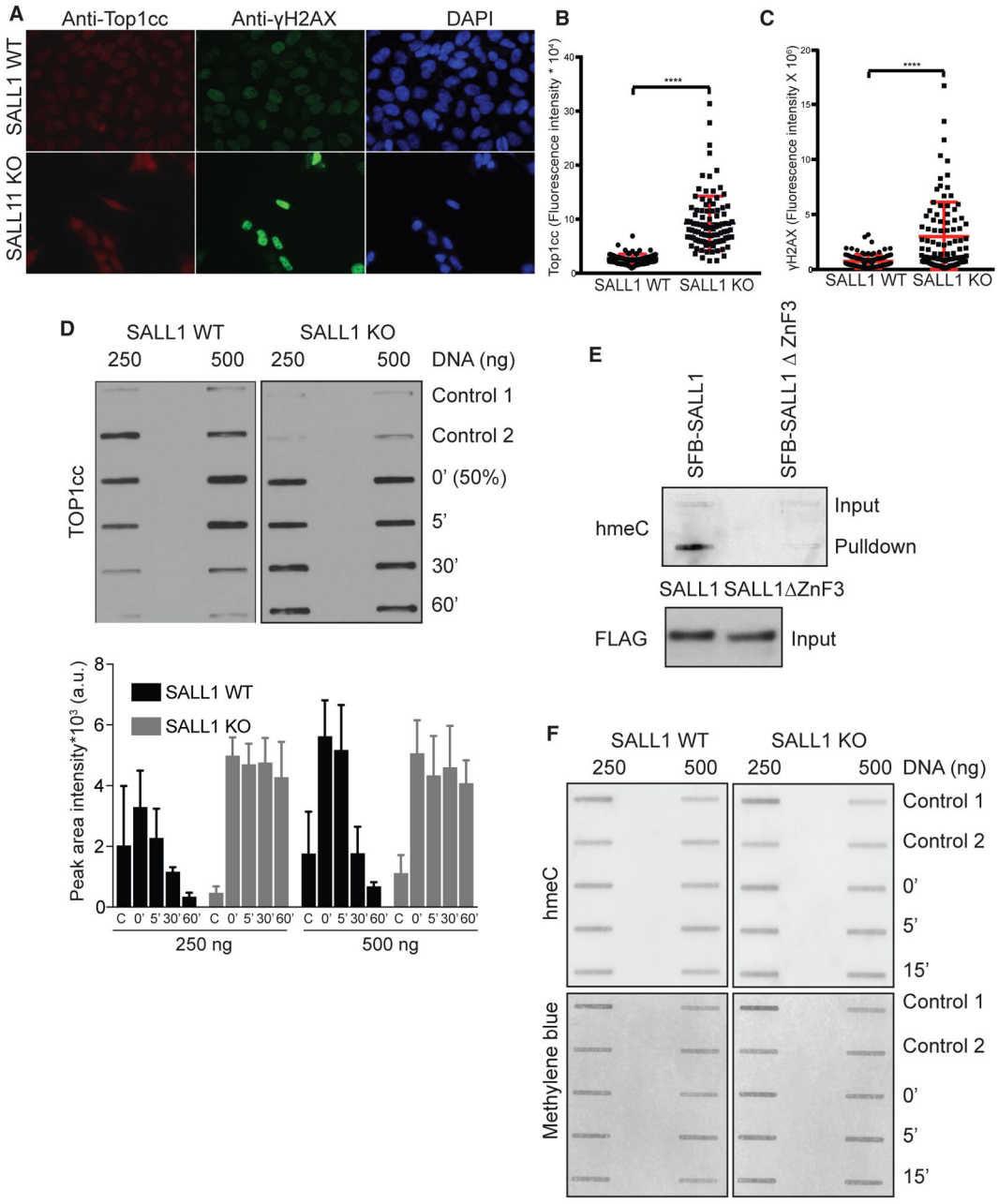

Figure 7. Role of SALL1 in Top1cc Resolution

(A) Immunofluorescence showing increased levels of covalently crosslinked Top 1 (Top1cc) after 15 min of recovery after 1 hr of CPT treatment (1 μM). Cells were also co-stained with γH2AX to observe levels of DNA damage and/or replication stress.

(B and C) Quantification of relative intensity of Top1cc adducts (B) and γH2AX(C) in 293A WT and SALL1-KO cells. Data are presented as mean ± SEM (****$p < 0.0001$).

(D) Slot-blot analysis showing the kinetics of Top1cc resolution after CPT treatment. Methylene blue staining shows the amount of DNA loaded in each sample. The SEM from three independent experiments is indicated. Total DNA was used for normalization for quantifications.

(E) Pull-down of SFB-SALL1 and SFB-SALL1ΔZn3 after their transient expression in HEK293T cells. Pulled-down DNA was quantitated, and an equal amount was loaded to determine the levels of hmeC in each sample with the use of anti-hmeC antibody.
(F) Slot blotting was performed to determine the levels of hmeC in 293A WT and SALL1-KO cel1s after treatment with CPT and during recovery phase (at 5, 10, and 15 min). Methylene blue staining was used to show equal amounts of loaded DNA.
See also Figure S7.

KEY RESOURCES TABLE

REAGENT or RESOURCE	SOURCE	IDENTIFIER
Antibodies		
Mouse monoclonal anti- Flag (M2)	Sigma-Aldrich	Cat#F3165; RRID:AB_262044
Mouse monoclonal anti- Vinculin	Sigma-Aldrich	Cat#V9131; RRID:AB_477629
Mouse monoclonal anti- PCNA (P10)	Cell Signaling Technology	Cat#2586S; RRID:AB_2160343
Rabbit polyclonal anti-WIZ	Atlas antibodies	Cat#HPA023774, RRID:AB_2671308
Rabbit monolyclonal anti-G9a	Cell Signaling Technology	Cat#3306S; RRID:AB_2097647
Rat monolyclonal anti-RPA32	Cell Signaling Technology	Cat#2208S; RRID:AB_2238543
Rabbit polyclonal anti-H3	Cell Signaling Technology	Cat#9715; RRID:AB_331563
Mouse monoclonal anti-BrdU (B44)	Becton Dickinson and Company	Cat#347580; RRID:AB_10015219
Mouse monoclonal anti-POLD1	Santa Cruz Biotechnology	Cat#sc-17776; RRID:AB_675487
Rabbit polyclonal anti-POLH	Abcam	Cat#ab186677; RRID:AB_2756352
Mouse monoclonal anti-RAD51	Santa Cruz Biotechnology	Cat#sc-398587; RRID:AB_2756353
Mouse monoclonal anti-Top1cc	EMD Millipore	Cat#MABE1084; RRID:AB_2756354
Rabbit polyclonal anti-hmeC	Active Motif	Cat#39770; RRID:AB_10013602
Rabbit polyclonal anti-γ-H2AX (S139)	Cell Signaling Technology	Cat#2577S; RRID:AB_2118010
Rabbit polyclonal anti-PARP1	Cell Signaling Technology	Cat#9542S; RRID:AB_2160739
Bacterial and Virus Strains		
Subcloning Efficiency DH5a Competent cells	Thermo Fisher Scientific	Cat#18265017
One Shot Stbl3 Chemically Competent Cells	Thermo Fisher Scientific	Cat#C737303
Chemicals, Peptides, and Recombinant Proteins		
Puromycin	Sigma-Aldrich	Cat#P8833
Pen-strep	Sigma-Aldrich	Cat#P4333
Biotin	Sigma-Aldrich	Cat#B4639
Deposited Data		
Raw mass spectrometry data	This paper	ProteomeXchange Consortium PRIDE: PXD011727
Experimental Models: Cell Lines		
HEK293T	ATCC	Cat#CRL-3216
HEK293A	ATCC	Cat#CRL-1573
Oligonucleotides		
sgRNA sequences for WIZ listed in table S7	This study	N/A
sgRNA sequences for SALL1 listed in table S7	This study	N/A
sgRNA sequences for G9a listed in table S7	This study	N/A
Recombinant DNA		

REAGENT or RESOURCE	SOURCE	IDENTIFIER
Gateway pDONR221	Thermo Fisher	Cat#12536017
pDEST-SFB	This study	N/A
pcDNA3.1 Myc BioID	Addgene	Cat#35700
pENTR223.1 SALL1	Harvard PlasmID database	Cat#HsCD00295069
LentiCRISPRv2	Addgene	Cat#52961
Software and Algorithms		
STRING	Szklarczyk et al., 2015	https://string-db.org
Genemania	Warde-Farley et al., 2010	https://genemania.org
TCGA: Cancer genome atlas	TCGA research network	http://cancergenome.nih.gov
CRAPome	Mellacheruvu et al., 2013	http://crapome.org